Polymer Chemistry



PAPER



Cite this: Polym. Chem., 2017, 8, 1699

Functional sugar-based polymers and nanostructures comprised of degradable poly(D-glucose carbonate)s†

Lu Su,^a Sarosh Khan,^a Jingwei Fan,^a Yen-Nan Lin,^{a,b} Hai Wang,^a Tiffany P. Gustafson,^a Fuwu Zhang^a and Karen L. Wooley*^a

Fundamental synthetic methodology was advanced to allow for the preparation of a reactive glucosebased block copolycarbonate, which was conveniently transformed into a series of amphiphilic block copolymers that underwent aqueous assembly into functional nanoparticle morphologies having practical utility in biomedical and other applications. Two degradable p-glucose carbonate monomers, with one carrying alkyne functionality, were designed and synthesized to access well-defined block polycarbonates (D < 1.1) via sequential organocatalytic ring opening polymerizations (ROPs). Kinetic studies of the organocatalyzed sequential ROPs showed a linear relationship between the monomer conversion and the polymer molecular weight, which indicated the controlled fashion during each polymerization. The pendant alkyne groups underwent two classic click reactions, copper-catalyzed azide-alkyne dipolar cycloaddition (CuAAC) and thiol-yne addition reactions, which were employed to render hydrophilicity for the alkyne-containing block and to provide a variety of amphiphilic diblock poly(p-glucose carbonate)s (PGCs). The resulting amphiphilic PGCs were further assembled into a family of nanostructures with different sizes, morphologies, surface charges and functionalities. These non-ionic and anionic nanoparticles showed low cytotoxicity in RAW 264.7 mouse macrophage cells and MC3T3 healthy mouse osteoblast precursor cells, while the cationic nanoparticles exhibited significantly higher IC₅₀ (162 μg mL⁻¹ in RAW 264.7; 199 μg mL⁻¹ in MC3T3) compared to the commercially available cationic lipid-based formulation, Lipofectamine (IC_{50} = 31 μ g mL⁻¹), making these nanomaterials of interest for biomedical applications.

Received 11th November 2016, Accepted 6th February 2017 DOI: 10.1039/c6py01978a

rsc.li/polymers

Introduction

The development of well-defined degradable polymers containing diverse functional groups and derived from bio-based feedstocks is of great interest, as the need for high performance, sustainable materials continues to rise. Such materials are designed to break down to regenerate biologically and environmentally resorbable natural products under normal or extreme conditions. The bio-derived building blocks are also expected to relieve dependence on petrochemical feedstocks. To date, there have been limited reports of the synthesis and post-polymerization modification of such polymers, among which aliphatic naturally-derived polycarbonates have received

In our continued efforts towards the development of functional renewable materials, ⁸⁻¹⁰ we have explored a glucose-based bicyclic carbonate that undergoes organocatalyzed ring opening polymerization (ROP) to yield either homopolymer poly(p-glucose carbonate)s (PGCs)¹¹ or diblock copolymers with a PGC connected to a biocompatible polyphosphoester (PPE) segment. ¹² Those PGCs are particularly attractive, as they originate from a renewable source and are able to break down into carbon dioxide and the protected (1,2,3-O-methyl protected) saccharide. However, the stability of methyl protecting groups and their lack of functionality limit the applications of the initially reported PGCs.

Herein, we designed and synthesized two glucose-based bicyclic carbonate monomers having carbonate protecting groups in the 2- and 3-positions: one carrying an alkyne functionality for further chemical manipulation via click chemistry and the other with two ethyl carbonate groups that can be degraded into methyl α -p-glucopyranoside, ethanol and carbon

considerable attention, due to their low toxicity, hydrolytic and enzymatic degradability, biocompatibility and potential biomedical application. 7

^aDepartments of Chemistry, Chemical Engineering and Materials Science & Engineering, Texas A&M University, College Station, Texas 77842, USA. E-mail: wooley@chem.tamu.edu

^bCollege of Medicine, Texas A&M University, Bryan, Texas 77807, USA

 $[\]dagger$ Electronic supplementary information (ESI) available: Experimental section and additional data. CCDC 1514598. For ESI and crystallographic data in CIF or other electronic format see DOI: 10.1039/c6py01978a

dioxide. Sequential ROPs of these two monomers provided access to well-defined natural product-based diblock copolymers. The polymerization behavior and kinetics of organocatalyzed sequential ROPs were comprehensively evaluated. The regiochemical and physicochemical properties of the resulting polymers were further studied by ¹³C NMR, thermogravimetric analysis (TGA) and differential scanning calorimetry (DSC). Rapid and efficient functionalization of the diblock PGCs was accomplished through copper-catalyzed azide-alkyne dipolar cycloaddition (CuAAC) and thiol-yne addition click reactions along the poly(methyl-2-O-ethyloxycarbonyl-3-O-propargyloxycarbonyl-4,6-O-carbonyl-α-D-glucopyranoside) [PGC(EPC)] segment to afford three different amphiphilic diblock PGCs. Those resulting amphiphilic diblock PGCs underwent assembly in aqueous solutions to generate a family of nanostructures with tunable surface properties. We expected that supramolecularassembly of the diblock PGCs would yield micelles and vesicles, with the advantage over the previous PPE-b-PGC by avoiding ethylene glycol as a degradation product.¹³ Rather, the degradation products from these polymers should include predominantly carbon dioxide, ethanol and methyl α-D-glucopyranoside, with additional lesser amounts of propargyl alcohol and products from the functionalized side chains. Cytocompatibility studies with RAW 264.7 mouse macrophage cells and MC3T3 healthy mouse osteoblast precursor cells were performed to elucidate the suitability of these polymers for in vivo use.

Results and discussion

Monomer design, synthesis and polymerization

Carbohydrates constitute an ideal renewable source for polymer building blocks, due to their rich structural variety and stereochemical diversity. 14-16 Glucose is one of the simplest carbohydrates and is abundant in Nature in both monomeric and polymeric forms.¹⁷ In order to incorporate glucose as the backbone building block of polymers that include carbonates, rather than biologically-based glycosidic bonds, the commercially available methyl-4,6-O-benzylidene-α-D-glucopyranoside (MBGlc) was chosen as the starting material. With its functionality and property conveniently controlled by manipulation of the pendant OH groups on the 2- and 3-positions, followed by removal of the benzylidene and installation of a 4,6-cyclic carbonate, two bicyclic carbonate monomers were designed from MBGlc. Importantly, each of two types of side chain groups were installed via alkoxycarbonyloxy linkages to provide protection of the 2- and 3-hydroxyl groups during controlled ROP, while later imparting specific properties to the polymers, and finally being capable of cleavage by hydrolysis. To maintain the functionality and self-assembly ability of the resulting block copolymers, one group contained a reactive chemical functionality that would be stable during polymerization and then readily available for chemical modification, and the other provided hydrophobicity.

Iadonisi and co-workers¹⁸ reported a facile and efficient approach to install alkoxycarbonyl protecting groups on carbohydrates by reaction with the corresponding chloroformates in the presence of tetramethylethylene diamine (TMEDA) at low temperature, and further demonstrated modulation of the reaction conditions to attain regioselective protection. Using this methodology, two monomers with ethyl carbonate or propargyl carbonate protecting groups in both C2 and C3 of MBGlc were synthesized and polymerized successfully by ROP without interference from transesterification reactions. However, since it was observed that the cyclic carbonate having two propargyl carbonate protecting groups in both C2

Scheme 1 Synthesis of bicyclic glucose-based carbonate monomer 4, methyl-2-O-ethyloxycarbonyl-3-O-propargyloxycarbonyl-4,6-O-carbonyl- α -D-glucopyranoside [GC(EPC)], and monomer 7, methyl-2,3-O-ethyloxycarbonyl-4,6-O-carbonyl- α -D-glucopyranoside [GC(EPC)].

Fig. 1 Single-crystal X-ray structure of 4 with key atoms labelled.

and C3 did not undergo controlled ROP, due to its poor solubility in dichloromethane (DCM), monomer 4 (GC(EPC)) with a propargyl carbonate in C3 and an ethyl carbonate in C2 was

developed. As shown in Scheme 1, good regioselectivity was obtained when MBGlc was treated with 1.1 equiv. of ethyl chloroformate and 0.6 equiv. of TMEDA at low temperature (-78 °C) since the OH group in C2 is more reactive than that in C3 at −78 °C. The structure of 1 was confirmed by X-ray diffraction (XRD) (Fig. S1†). Further modification of C3 with propargyl chloroformate was carried out in an ice bath in quantitative yield within 1 h. Subsequent removal of the benzylidene group via acid-catalyzed hydrolysis and formation of the bicyclic monomer with triphosgene gave 4 in 56% yield after column chromatography and 42% yield following recrystallization in hexanes/ethyl acetate. The structure of 4 was confirmed by ¹H NMR, ¹³C NMR, COSY, HMQC, HMBC and FT-IR spectroscopies as well as by electrospray ionization mass spectrometry (ESI-MS) analysis (Fig. S2-S4†). A single crystal of 4 was analyzed by XRD, which further confirmed the regioselective structure (Fig. 1). Similarly, monomer 7 with two ethyl carbonate protecting groups was synthesized in three steps with an overall yield of 41% (Scheme 1) and was characterized using the same methods (Fig. S5-S7†).

Scheme 2 Synthesis of PGC(EPC), PGC(EC) and PGC(EPC)-b-PGC(EC) via organocatalytic ROPs.

Table 1 Polymerization of GC(EPC) catalyzed by TBD and DBU under different conditions

Entry	Cat.	T (°C)	[M]:[I]	Time (min)	Conv. ^a	$M_{\mathrm{n\ NMR}}^{b}(\mathrm{kDa})$	D^{c}
1	TBD	25	50:1	1.5	85%	15.8	1.10
2	TBD	25	50:1	3	97%	18.0	1.20
3	TBD	-78	50:1	1.5	82%	15.2	1.04
4	TBD	-78	50:1	3	95%	17.8	1.05
5	DBU	25	50:1	16	99%	18.3	1.07
6	DBU	25	20:1	15	99%	7.5	1.06
7	DBU	25	100:1	30	93%	34.6	1.12

The initiator was 4-methylbenzyl alcohol and the solvent was anhydrous DCM for all entries. Organocatalyst was 2 mol% to monomer for all entries. a Conversion (conv.) was determined by the relative integration of the monomer and polymer RI signals in the THF SEC chromatogram. ${}^bM_{\rm n~NMR}$ was calculated from the integral of the methyl protons originating from the initiator with that of the proton at the anomeric carbon, based on 1 H NMR spectra of final polymer products. cD was measured by THF SEC calibrated using polystyrene standards.

The organocatalytic ROP of GC(EPC) was investigated with 1,5,7-triazabicyclo-[4.4.0]dec-5-ene (TBD) and 1,8-diazabicycloundec-7-ene (DBU) catalysts (Scheme 2, Table 1), which had previously shown excellent control in the ROP of carbonate monomers. 11,19 Initially, TBD was employed to catalyze the polymerization of GC(EPC) initiated by 4-methylbenzyl alcohol at room temperature (entries 1 and 2 of Table 1). The polymerization of GC(EPC) reached over 85% conversion within only 1.5 min with molecular weight distributions (D) < 1.2, indicating good control. However, broadening of the D (1.18–1.3)

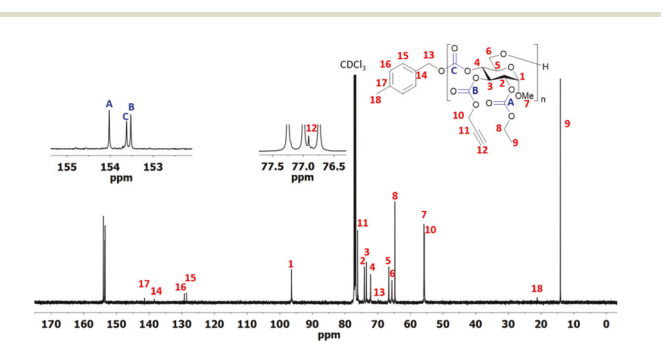


Fig. 2 ¹³C NMR spectrum of PGC(EPC) in CDCl₃.

when the conversion reached 97% indicated the occurrence of adverse backbiting or transesterification reactions of the polymer backbone. Therefore, the reaction temperature was decreased (entries 3 and 4 of Table 1) and TBD was replaced by the less active catalyst DBU (entries 5–7 of Table 1) to access narrower D. These polymerizations appeared to be kinetically controlled, as decreasing the temperature ($-78~^{\circ}$ C) had no effect on reaction time, but led to narrower D (1.03-1.07). The use of DBU also yielded narrower D (1.06-1.12) compared to polymerizations with TBD as the catalyst. The catalytic behavior of DBU in the polymerization of 4 was further studied by tuning the monomer-to-initiator molar ratio (entries 5–7 of Table 1). The molecular weight distributions were all less than 1.12 and the size exclusion chromatography (SEC) traces were symmetrical and unimodal.

The structure of PGC(EPC) was confirmed by FT-IR, ¹H NMR (Fig. S8†) and ¹³C NMR spectroscopies (Fig. 2). The ¹³C NMR spectrum showed the characteristic resonance for the backbone carbonate linkage at 153.6 ppm, confirming the head-to-tail (HT) regioselectivity of the PGCs. As ether-protected poly(sugar carbonate)s developed previously by the Wooley¹¹ and Gross²⁰ groups both showed regiorandom structures, we hypothesized that the carbonate protecting groups may further coordinate with TBD or DBU to selectively open

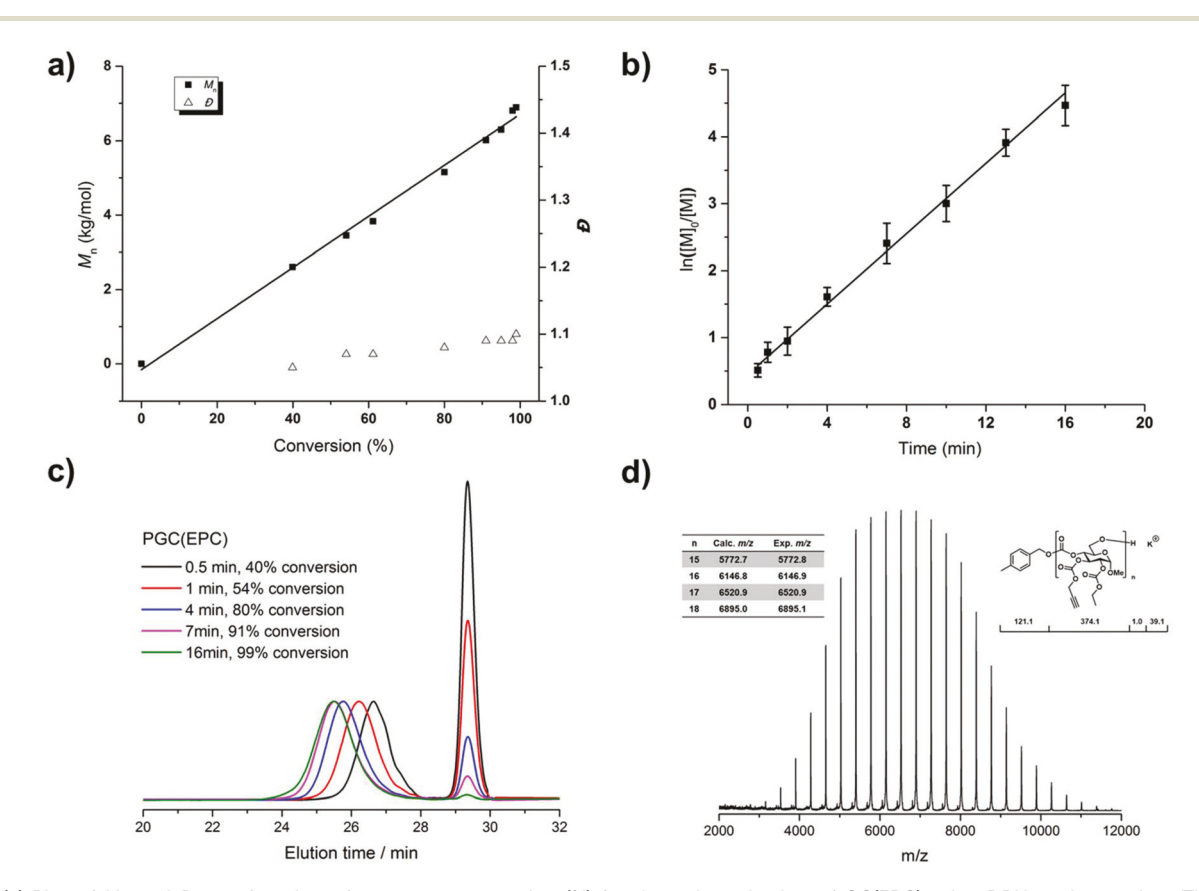


Fig. 3 (a) Plot of M_n and D as a function of monomer conversion (%) for the polymerization of GC(EPC) using DBU as the catalyst. The ratio of monomer: initiator: DBU was 50:1:1. (b) Kinetic plots of monomer conversion ($\ln([M]_0/[M])$) as a function of time using data obtained by SEC (RI detector). (c) SEC traces (THF as eluent, 1 mL min⁻¹) of the ROP of 4 as a function of polymerization time, with normalization of the intensity of the polymer peaks. (d) MALDI-Tof MS spectrum of PGC(EPC) ($DP_n = 18$ by 1 H NMR spectroscopy).

the cyclic monomer in a regioregular fashion. Such coordination may also explain the similar reaction times required for quantitative monomer conversion at -78 and 25 °C. The regioselectivity was also achieved by ROP of D-mannose carbonate reported recently by Buchard and co-workers, arising from the additional steric constraint imposed by the 2,3-O-isopropylidene protecting group.²¹ XRD of bulk and annealed PGC(EPC) samples was performed to determine the impact of the regioregular structure on polymer segment alignment. The XRD spectra showed a broad halo rather than a sharp reflection peak (Fig. S9†) in both bulk and annealed samples, indicating the amorphous characteristic of these polymers. Its mannose counterpart, the regioregular poly(p-mannose carbonate)s also showed no sign of crystallinity.²¹ Thermal properties were evaluated by TGA and DSC. The glass transition temperature (T_{o}) of PGC(EPC) was above 100 °C even for polymers with low molecular weights (entry 6 of Table 1), which likely arose from the cyclic structure in the backbone.

We studied the kinetics of ROP of 4 using a monomer/ initiator feed ratio ([M]₀/[I]₀) of 50 in DCM with 4-methylbenzyl alcohol as the initiator and DBU as the organocatalyst to allow for monitoring of the monomer conversion and the growth of the polymer chains as a function of time. Monomer conversion was determined by comparing the integration of their refractive index (RI) signals between polymer and monomer (peak in 29.3 min) in SEC traces (Fig. 3c). The number-average molecular weights (M_n) were calculated using ¹H NMR spectra after isolation of the polymer samples by precipitation, with comparison of the integral of the methyl protons originating from the initiator with that of the proton at the anomeric carbon. The linear relationship between M_n and monomer conversion suggested a well-controlled polymerization. The conversion of 4 reached 99% within 16 min (Fig. 3a). The SEC traces showed unimodal peaks during the reaction, which shifted toward shorter elution times as polymerization progressed while maintaining narrow D values below 1.1 (Fig. 3a and c). Linear plots of $ln([M]_0/[M])$ vs. time (Fig. 3b) also indicated that the polymerization occurred in a controlled manner as expected from ROP.²²

Analysis of a low molecular weight polymer ($DP_n = 18$ by 1H NMR spectroscopy) by matrix-assisted laser desorption ionization time-of-flight mass spectrometry (MALDI-Tof MS) revealed two populations, each with a spacing of 374.1 m/z equal to that of the expected monomer repeat unit (Fig. 3d). Structurally, these two sets of signals corresponded to populations with distinct end groups, *e.g.*, a major population initiated by 4-methylbenzyl alcohol and a minor population initiated by water (trace water contaminant). The main peak at m/z = 6520.9 corresponded to a potassium-charged polymer chain of $DP_n = 17$ with a methylbenzyloxy and protonated α - and ω -end groups, respectively, in the major population, further confirming the living nature of the polymerization.

Chain extension with a second monomer, 7, was achieved *via* one-pot sequential ROPs with DBU as the organocatalyst at room temperature (Scheme 2). The concentration of the second monomer decreased from 0.5 M to 0.25 M, resulting in

slower polymerization rate and lower monomer conversion. No higher than 90% monomer conversion was achieved even with 40 min reaction time, compared with the first block that reached 99% conversion in 16 min. The block copolymer PGC (EPC)-*b*-PGC(EC), 8, was characterized by a combination of data obtained from SEC, ¹H NMR, TGA and DSC (Fig. S10–S12†). The block copolymer peak in the SEC trace shifted toward shorter elution time compared to the first block PGC

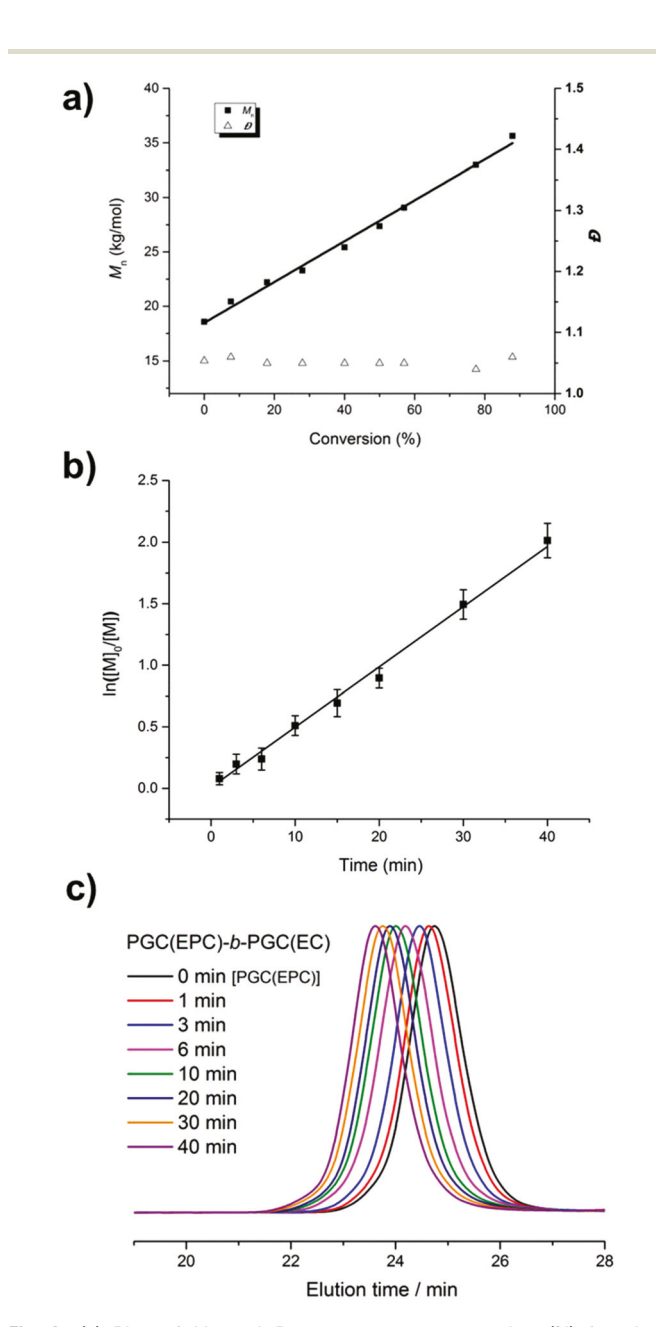


Fig. 4 (a) Plot of M_n and $\mathcal D$ vs. monomer conversion (%) for chain extension of PGC(EPC) with GC(EC) via sequential ROPs. Conditions: [GC(EC)] = 0.25 M in DCM, [GC(EC)] : [PGC(EPC)] = 50 : 1. (b) Kinetic plots of monomer conversion (ln([M] $_0$ /[M])) vs. time. (c) SEC traces (THF as eluent, 1 mL min $^{-1}$) as a function of polymerization time, for the chain extension of PGC(EPC) with GC(EC) upon addition of a solution of GC (EC) in DCM at 16 min after initiation of the homopolymerization of GC (EPC).

(EPC), correlating with increased molecular weight measured by 1 H NMR, and showed narrow D (<1.1). DSC revealed a high $T_{\rm g}$ to be 114 $^{\circ}$ C. This one-pot sequential synthesis of well-defined diblock PGCs is more advantageous than the chain extension from purified macroinitiator.

Chain extension with 7 was achieved within 40 min with good control. A linear plot of M_n vs. monomer conversion was observed during polymerization, which reached 90% conversion and resulted in low D (<1.1) (Fig. 4a). Similar as the homopolymerization of 4, the kinetic plots of $\ln([M]_0/[M])$ vs. time for GC(EC) chain extension showed pseudo-first-order kinetics (Fig. 4b). The SEC peaks shifted toward shorter elution times as chain extension progressed, maintaining D values below 1.1 (Fig. 4c).

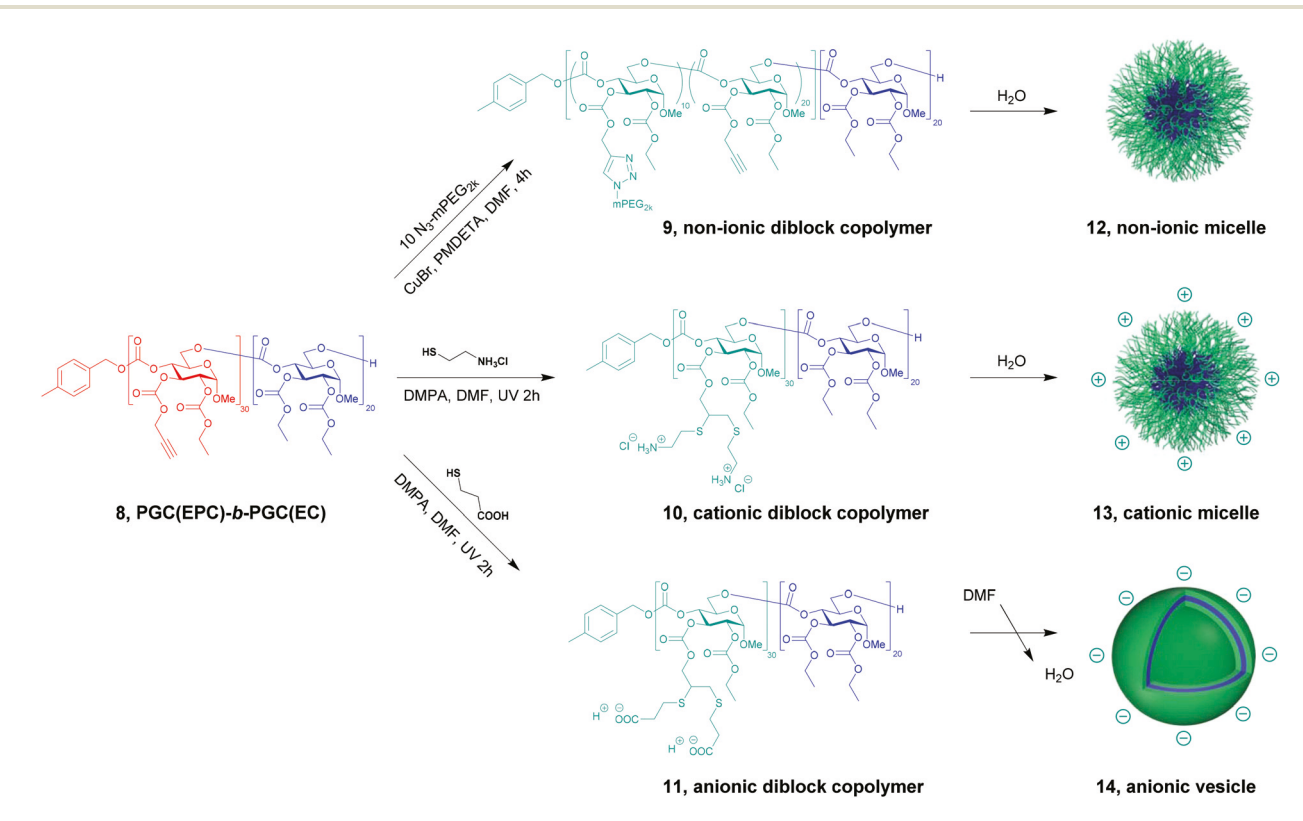
Functionalization of alkyne-containing block copolymers by CuAAC and radical thiol-yne addition reactions

The alkyne-containing diblock polycarbonates were further functionalized by CuAAC with ${\rm CH_3O\text{-}PEG_{2k}\text{-}azide}$ (Scheme 3). PEG was selected for addition onto the diblock PGCs due to its extensive use in biomaterials owing to its high hydrophilicity, biocompatibility and anti-fouling properties. ^{23,24} PEGylation was achieved as confirmed by ¹H NMR spectroscopy, by the appearance of a new resonance consistent with the triazole proton at 7.85 ppm and PEG resonances at 3.71–3.61 and 3.40 ppm (Fig. S13†). The resonance attributed to the residual acetylene protons at 2.60 ppm was broadened, likely due to the

presence of surrounding PEG chains. SEC analysis of the PEGylated diblock PGCs **9** in Fig. 5 revealed a shift to lower retention time while maintaining a narrow dispersity, similar to that of the unmodified diblock PGCs (pre-modification: $M_n = 16\,300 \text{ g mol}^{-1}$, D = 1.05; post-modification: $M_n = 31\,200 \text{ g mol}^{-1}$, D = 1.16). Furthermore, the residual alkyne groups can be utilized for subsequent crosslinking or modification with other functional molecules, *e.g.*, dyes, which is currently underway in our group.

Thiol-yne chemistry was performed as an alternative postpolymerization technique for the functionalization of the
pendant alkyne groups (Scheme 3). A total of 20 equiv. of
thiol, 2-aminoethanethiol hydrochloride or 3-mercaptopropionic acid, were used relative to alkynes in the radical reaction to
avoid cross-linking and ensure high efficiency. The complete
disappearance of the terminal acetylene protons (2.60 ppm)
observed in the ¹H NMR spectra of the two resulting polymers 10 and 11, suggested full consumption of the alkynes.
Additionally, the presence of other functional groups verified
the successful installation of the two different thiols onto the
diblock PGCs (Fig. S14 and S15†). FT-IR spectroscopy confirmed the consumption of the terminal alkynes and the introduction of the desired amines and carbonyl groups (Fig. S16†).

Post-polymerization functionalization of the pendant alkyne groups on PGCs *via* CuAAC and thiol-yne reactions showed to be highly efficient without observable polymer degradation, and transformed the hydrophobic diblock copoly-



Scheme 3 Schematic representation of the functionalization of $PGC(EPC)_{30}$ -b- $PGC(EC)_{20}$ by CuAAC with CH_3O - PEG_{2k} -azide and radical thiol-yne addition with 2-aminoethanethiol hydrochloride or 3-mercaptopropionic acid, and subsequent self-assembly of the three resulting amphiphilic diblock PGCs.

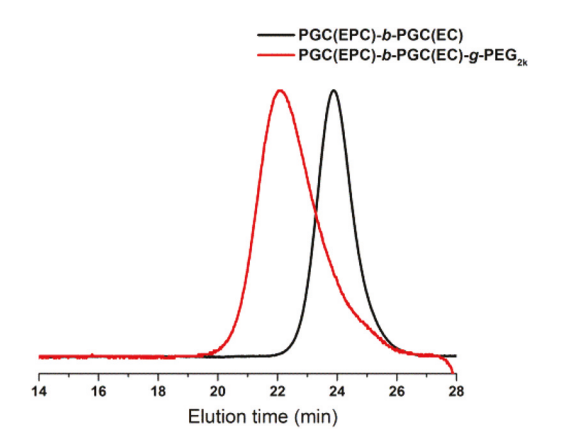


Fig. 5 SEC traces of diblock copolymer PGC(EPC)-b-PGC(EC), **8**, and modified polymer PGC(EPC)-b-PGC(EC)-g-PEG_{2k}, **9**.

mer into three different amphiphilic PGCs 9, 10 and 11. The versatility of functionalization makes these polymer scaffolds an appealing platform for the facile preparation of new functional degradable and biocompatible materials.

Self-assembly of amphiphilic diblock PGCs

The self-assembly behavior of the amphiphilic diblock copolymers was evaluated by either direct re-suspension of lyophilized polymers into nanopure water or by addition of nanopure water into an organic solution of polymer. The non-ionic

PGCs 9 and positively-charged PGCs 10 were dissolved in nanopure water by sonication for 10 min at room temperature. Transmission electron microscopy (TEM) and dynamic light scattering (DLS) showed the non-ionic and cationic block PGCs spontaneously formed spherical nanoparticles with narrow size distributions (Fig. 6). However, the negatively-charged PGCs 11 were not able to be directly suspended into water. Rather, the corresponding anionic nanoparticles were prepared by adding nanopure water into the DMF solution of the polymer, followed by further dialysis against nanopure water.

In the nanoparticle assemblies, it is expected that the hydrophobic PGC(EC) block would aggregate in the particle core and be shielded from the aqueous medium by the shell region consisting of functionalized PGC(EPC) blocks, due to the highly hydrophilic nature of the PEG_{2k}, carboxylate and amino groups. The morphological influence of varying the PGC(EPC) block functionalities on the self-assembled nanostructures was characterized by TEM and DLS. TEM revealed micellar structures 12 and 13 with number-average diameter (D_{av}) of ca. 13 and 19 nm, originating from assembly of 9 and 10, respectively, while vesicular structures 14 were observed with D_{av} of ca. 120 nm from assembly of 11 (Fig. 6a, c, and e). The differences in morphology could be explained as being due to the low pH value of nanopure water (ca. 5.5), which would lead to a lower hydrophilic-hydrophobic ratio for the carboxylic acid-containing anionic polymer, relative to those of the non-ionic and cationic polymers. Therefore, vesicles

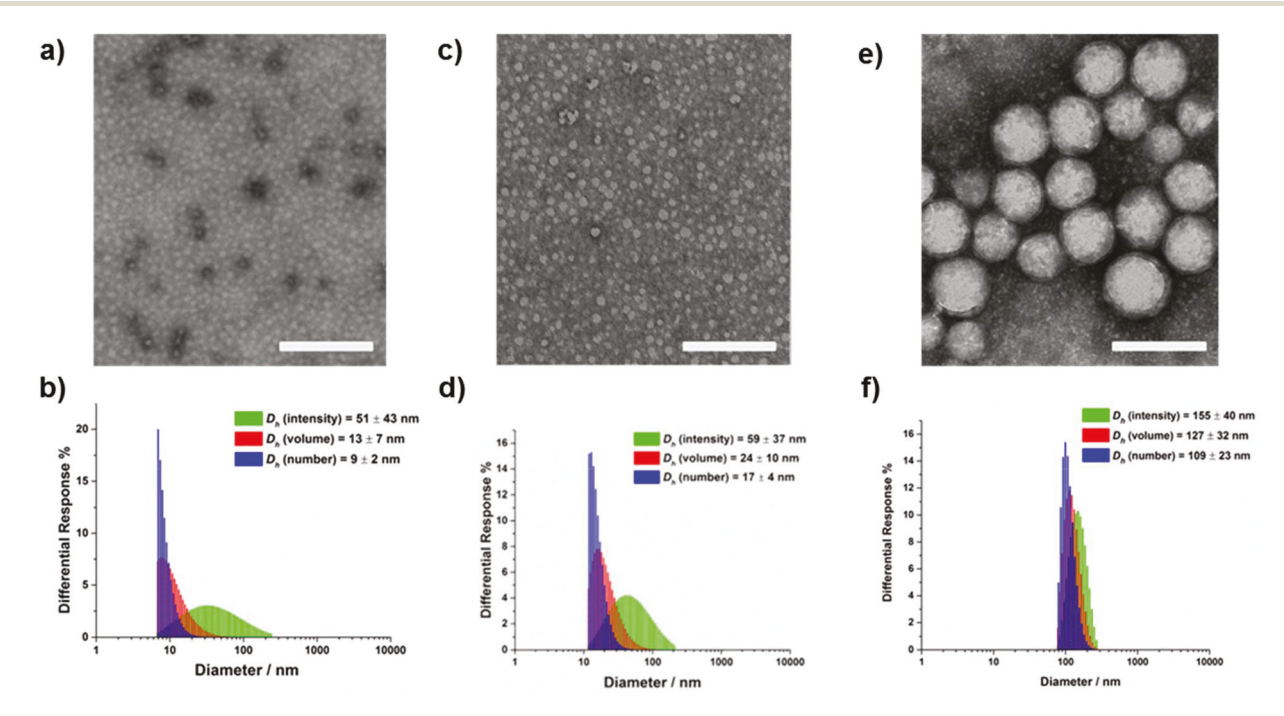


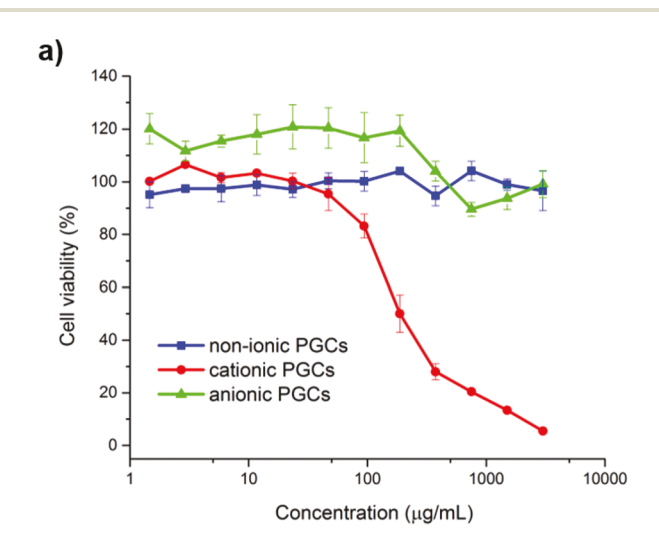
Fig. 6 Self-assembly results of non-ionic micelle, cationic micelle and anionic vesicle in nanopure water. (a) TEM images of $\mathbf{12}$: $D_{\text{av}} = 13$ nm, after counting more than 100 nanoparticles. (b) DLS results of $\mathbf{12}$: $D_{\text{h(intensity)}} = 51 \pm 43$ nm, $D_{\text{h(volume)}} = 13 \pm 7$ nm, $D_{\text{h(number)}} = 9 \pm 2$ nm. (c) TEM images of $\mathbf{13}$: $D_{\text{av}} = 19$ nm, after counting more than 100 nanoparticles. (d) DLS results of $\mathbf{13}$: $D_{\text{h(intensity)}} = 59 \pm 37$ nm, $D_{\text{h(volume)}} = 24 \pm 10$ nm, $D_{\text{h(number)}} = 17 \pm 4$ nm. (e) TEM images of $\mathbf{14}$: $D_{\text{av}} = 120$ nm, after counting more than 100 nanoparticles. (f) DLS results of $\mathbf{14}$: $D_{\text{h(intensity)}} = 155 \pm 40$ nm, $D_{\text{h(volume)}} = 127 \pm 32$ nm, $D_{\text{h(number)}} = 109 \pm 23$ nm. All scale bars in TEM images are 200 nm.

formed from anionic diblock PGCs **11**. DLS showed unimodal size distributions of particles formed from all of the amphiphilic PGCs. The number-average hydrodynamic diameter values $[D_{h(number)}]$ of **12**, **13**, and **14** were 9 \pm 2, 17 \pm 4, and 109 \pm 23 nm, respectively (Fig. 6b, d, and f).

The surface charge densities were characterized by ζ -potential measurements in nanopure water at pH 5.5. Non-ionic micelles 12 were slightly negatively charged with ζ -potential of -4 ± 1 mV, which is commonly observed for neutral polymer nanoparticles. 25,26 ζ -Potential values of 47 \pm 2 mV and -41 ± 1 mV indicated the cationic and anionic surface characteristics of the self-assembled nanoparticles 13 and 14, respectively.

Cytotoxicity of PGC nano-materials

Nanoparticles were then tested for their toxicity in the cancer cell line, RAW 264.7 mouse macrophage, and healthy cell line, MC3T3 mouse osteoblast precursor cells, at a concentration range of 1.5–3000 μg mL⁻¹ (Fig. 7). Non-ionic and anionic



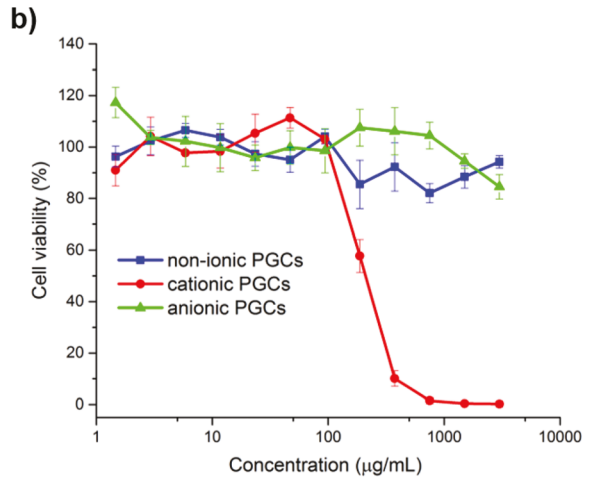


Fig. 7 Cytotoxicity of the non-ionic, cationic, and anionic nanoparticles in the RAW 264.7 mouse macrophage cell line (a) and the MC3T3 mouse osteoblast precursor cell line (b) after treatment with PGC nanostructures at concentrations ranging from 1.5–3000 $\mu g\ mL^{-1}$ for 24 h.

nanoparticles showed no observable cytotoxicity over the tested concentration range in both cell lines. Compared with previously reported anionic polymers that showed significant cytotoxicity towards the RAW 264.7 mouse macrophages cell line at concentrations above 1 mg mL⁻¹, ²⁷ the anionic nanoparticles were not cytotoxic at concentrations of 1-3 mg mL⁻¹ and, in fact, exhibited cell proliferative activities at concentrations below 1 mg mL⁻¹. Further experiments are needed to decipher the mechanism of this phenomenon. Cationic nanoparticles showed a dose-dependent toxicity, likely due to electrostatic interactions with the negatively-charged cell membrane.²⁸ Cationic nanoparticles exhibited significantly higher IC_{50} (162 µg mL⁻¹ in RAW 264.7; 199 µg mL⁻¹ in MC3T3) compared to Lipofectamine (IC₅₀ = 31 μ g mL⁻¹), ²⁹ a commercially available cationic lipid-based formulation, highlighting the low cytotoxicity of our PGCs even with a cationic surface.

All experiments were performed according to institutional guidelines provided by Texas A&M's Environmental Health and Safety committee. Experiments involving mouse derived cell lines (RAW 264.7 and MC3T3) were performed according to guidelines provided by Texas A&M's Institutional Biosafety Committee for biosafety level 1 organisms (protocol approval number IBC2014-075).

Conclusions

PGC-based materials represent a new functional polymer platform prepared from renewable sources that can be rapidly transformed into a diverse variety of amphiphilic diblock copolymers, with the potential to break down into natural byproducts. By installing protecting groups as functional entities through labile linkages, these materials offer advances over our earlier poly(glucose carbonate) and polyphosphoester systems. We have designed and synthesized two degradable carbonate monomers with one containing alkyne functionality. The corresponding block PGCs were prepared via sequential ROPs occurring in a controlled manner, resulting in predictable molecular weights and narrow D. Notably, the postpolymerization modification of the pendant alkyne groups via CuAAC and thiol-yne addition reactions were highly efficient and proceeded without observable polymer degradation, providing a variety of amphiphilic diblock PGCs. Those diblock PGCs further assembled into a family of nanostructures with different sizes, morphologies, surface charges and functionalities, while maintaining alkynes in the hydrophilic domains for further chemical manipulations. Currently, we are exploring the degradable nanoparticles in various biomedical and agricultural applications.

Acknowledgements

We gratefully acknowledge financial support from the National Science Foundation [CHE-1410272 and CHE-1610311], and the Robert A. Welch Foundation (A-0001). We thank Dr Junsheng Qin

for X-ray characterization and analysis. The mass spectrometry facility at Texas A&M University is also gratefully acknowledged.

Notes and references

- 1 S. A. Miller, ACS Macro Lett., 2013, 2, 550-554.
- 2 R. Mülhaupt, Macromol. Chem. Phys., 2013, 214, 159-174.
- 3 S. D. Sommerfeld, Z. Zhang, M. C. Costache, S. L. Vega and J. Kohn, *Biomacromolecules*, 2014, **15**, 830–836.
- 4 S. Mecking, Angew. Chem., Int. Ed., 2004, 43, 1078-1085.
- 5 F.-T. Tsai, Y. Wang and D. J. Darensbourg, J. Am. Chem. Soc., 2016, 138, 4626–4633.
- 6 J. R. Lowe, M. T. Martello, W. B. Tolman and M. A. Hillmyer, *Polym. Chem.*, 2011, 2, 702–708.
- 7 S. Tempelaar, L. Mespouille, O. Coulembier, P. Dubois and A. P. Dove, *Chem. Soc. Rev.*, 2013, 42, 1312–1336.
- 8 S. Zhang, A. Li, J. Zou, L. Y. Lin and K. L. Wooley, ACS Macro Lett., 2012, 1, 328–333.
- 9 S. Zhang, J. Zou, F. Zhang, M. Elsabahy, S. E. Felder, J. Zhu, D. J. Pochan and K. L. Wooley, *J. Am. Chem. Soc.*, 2012, 134, 18467–18474.
- 10 J. Fan, R. Li, X. He, K. Seetho, F. Zhang, J. Zou and K. L. Wooley, *Polym. Chem.*, 2014, 5, 3977–3981.
- 11 K. Mikami, A. T. Lonnecker, T. P. Gustafson, N. F. Zinnel, P. J. Pai, D. H. Russell and K. L. Wooley, *J. Am. Chem. Soc.*, 2013, 135, 6826–6829.
- 12 T. P. Gustafson, A. T. Lonnecker, G. S. Heo, S. Y. Zhang, A. P. Dove and K. L. Wooley, *Biomacromolecules*, 2013, 14, 3346–3353.
- 13 S. Zhang, J. Zou, M. Elsabahy, A. Karwa, A. Li, D. A. Moore, R. B. Dorshow and K. L. Wooley, *Chem. Sci.*, 2013, 4, 2122– 2126.
- 14 E. L. Dane and M. W. Grinstaff, *J. Am. Chem. Soc.*, 2012, 134, 16255–16264.
- 15 C. R. Bertozzi and L. L. Kiessling, *Science*, 2001, **291**, 2357–2364.

- 16 J. A. Galbis, G. Garcia-Martin Mde, M. V. de Paz and E. Galbis, *Chem. Rev.*, 2016, **116**, 1600–1636.
- 17 A. J. Ragauskas, C. K. Williams, B. H. Davison, G. Britovsek, J. Cairney, C. A. Eckert, W. J. Frederick, J. P. Hallett, D. J. Leak, C. L. Liotta, J. R. Mielenz, R. Murphy, R. Templer and T. Tschaplinski, *Science*, 2006, 311, 484–489.
- 18 M. Adinolfi, G. Barone, L. Guariniello and A. Iadonisi, *Tetrahedron Lett.*, 2000, **41**, 9305–9309.
- 19 S. Tempelaar, L. Mespouille, P. Dubois and A. P. Dove, *Macromolecules*, 2011, 44, 2084–2091.
- 20 Y. Shen, X. Chen and R. A. Gross, *Macromolecules*, 1999, 32, 2799–2802.
- 21 G. L. Gregory, L. M. Jenisch, B. Charles, G. Kociok-Köhn and A. Buchard, *Macromolecules*, 2016, **49**, 7165–7169.
- 22 N. E. Kamber, W. Jeong, R. M. Waymouth, R. C. Pratt, B. G. G. Lohmeijer and J. L. Hedrick, *Chem. Rev.*, 2007, **107**, 5813–5840.
- 23 P. Caliceti and F. M. Veronese, *Adv. Drug Delivery Rev.*, 2003, 55, 1261–1277.
- 24 M. J. Roberts, M. D. Bentley and J. M. Harris, *Adv. Drug Delivery Rev.*, 2002, 54, 459–476.
- 25 S. K. Sahoo, J. Panyam, S. Prabha and V. Labhasetwar, I. Controlled Release, 2002, 82, 105–114.
- 26 L. Su, W. Y. Zhang, X. L. Wu, Y. F. Zhang, X. Chen, G. W. Liu, G. S. Chen and M. Jiang, *Small*, 2015, 11, 4191– 4200.
- 27 H. Zhang, X. Lin, S. Chin and M. W. Grinstaff, *J. Am. Chem. Soc.*, 2015, 137, 12660–12666.
- 28 S. Hong, P. R. Leroueil, E. K. Janus, J. L. Peters, M.-M. Kober, M. T. Islam, B. G. Orr, J. R. Baker and M. M. Banaszak Holl, *Bioconjugate Chem.*, 2006, 17, 728–734.
- 29 M. Elsabahy, S. Zhang, F. Zhang, Z. J. Deng, Y. H. Lim, H. Wang, P. Parsamian, P. T. Hammond and K. L. Wooley, *Sci. Rep.*, 2013, 3, 3313.